World Scientific
www.worldscientific.com

Piezoresponse force microscopy and dielectric spectroscopy study of $Ba_{0.6}Sr_{0.4}TiO_3$ thin films

Dionizy Czekaj* and Agata Lisińska-Czekaj

Department of Materials Engineering and Welding
Faculty of Mechanical Engineering
Gdańsk University of Technology
11/12, Narutowicza St., Gdańsk 80-233, Poland
*dioniziy.czekaj@pg.edu.pl

Research on synthesis, characterization and determination of processing — structure — property relationships of commercially important ferroelectric thin films has been performed. The sol–gel type solution deposition technique was applied to produce good quality thin films of $Ba_{0.6}Sr_{0.4}TiO_3$ (BST60/40) chemical composition on the stainless steel substrates. The thin films were characterized in terms of their microstructure, crystal structure, phase composition, piezoelectric and dielectric properties. It was found that the BST60/40 thin film adopted the cubic structure at room temperature with an elementary cell parameter $a = 3.971(8)$ Å. Morphology of the thin film surface was studied with Atomic Force Microscopy (AFM). Average roughness of the thin films surface was found ($Sa = 0.055\,\mu m$). Piezoresponse Force Microscopy (PFM) was applied for the thin film characterization. Active piezoelectric regions were found in BST60/40 thin film. Therefore, dielectric response measured at room temperature was studied in assumption of piezoelectric electric equivalent circuit.

Keywords: Thin film; $Ba_{0.6}Sr_{0.4}TiO_3$; crystal structure; dielectric spectroscopy; piezoresponse force microscopy.

1. Introduction

According to Landoldt and Börnstein[1,2] there are about 600 ferro- and anti-ferroelectric materials. However, there are a limited number of structures that are adopted by the majority of the commercially important ferroelectric oxides.[3] The main ferroelectric materials used in ferroelectric devices can be classified as ABO_3-type materials. It is well known that ABO_3 structure permits large variations in compositions by substitution on A-or B-sites by radius compatible ions.[4] Barium strontium titanate ($Ba_{1-x}Sr_x)TiO_3$ — BST) adopts the ABO_3-type structure.

The properties of $(Ba_{1-x}Sr_x)TiO_3$ are known to depend on the composition x.[3,4] The Curie temperature (T_C) and the relative dielectric constant (ε_r) of bulk BST vary from $T_C \sim 127°C$ to $T_C \sim -243°C$ and $\varepsilon_r \sim 2000$ to $\varepsilon_r \sim 300$, respectively, for x from 0.0 to 1.0. By adjusting the Ba/Sr ratio to be 73/27, Curie point of BST can be close to the room temperature.

It is also important to realize that thin film may differ in some substantial ways from bulk ceramics or single crystals of the same chemical composition.[5] One source of these differences is the substantial in-plane stress that thin films are typically under, ranging from MPa to GPa.[3] Because many ferroelectric materials are also ferroelastic, imposed stress can markedly affect the stability of the ferroelectric phase as well as the ease with which polarization can be reoriented in some directions.

The deposition of thin film functional layers on different substrates is an essential step for many fields of modern high technology.[6,7] Applications range from large area optical coatings on architectural structures to tribological layers, high-temperature superconductors, and finally to applications in micro and nanoelectronics.[3] Considering this broad spectrum of applications, it is obvious that there cannot be one perfect deposition method which can be applied in all fields.

The goal of the present research was focused on $(Ba_{0.6}Sr_{0.4})TiO_3$ electroceramic thin films grown on stainless steel substrates by the sol–gel type solution deposition technique followed by thermal processing, morphology studies (AFM/PFM), crystal structure and phase composition (X-ray diffraction method) and dielectric response studies.

2. Experimental

Barium acetate ($Ba(C_2H_3O_2)_2$), strontium acetate ($Sr(C_2H_3O_2)_2$) and tetrabutyl titanate ($Ti(OC_4H_9)_4$) were used as starting materials for the sol–gel type chemical solution deposition of $(Ba_{0.6}Sr_{0.4})TiO_3$ (BST60/40) thin films. Glacial acetic acid (CH_3COOH) was used as a catalyst, whereas *n*-butanol ($CH_3(CH_2)_3OH$) was used as a solvent.

All the above reagents were analytic in purity. After stoichiometrically dissolved, mixed and stirred, the precursor solution was deposited by spin coating on polished stainless steel substrates (AISI 304 type). Spin coating was performed at $\omega = 3500$ revolution per min for $t = 30$ s to form wet films. The wet films were given a heat treatment at $T = 150°$C for $t = 5$ min to remove H_2O, then pyrolyzed at $T = 350°$C for $t = 5$ min to form inorganic thin films. The coating process was repeated up to 15 or 30 times thus yielding thin films of $d = 300$ nm or $d = 600$ nm in thickness, respectively.

Final crystallization of as-deposited BST60/40 thin films was carried out in an ambient atmosphere at $T = 650°$C for 2 h (the heating rate was 1°C/min) by conventional furnace annealing.

The dry gel of BST60/40 chemical composition was analyzed by thermo-gravimetric analysis and by differential thermal analysis (DTA). Simultaneous measurements were executed in air by STA-409 Netzsch analyzer. Temperature rate was $v = 10°$C/min.

The crystal structure of BST60/40 electroceramic thin films was studied by X-ray diffraction method at room temperature (Philips PW 3710 X-ray diffractometer, Θ–2Θ mode, CoKα radiation, detector scan step $\Delta 2\Theta = 0.01°$ and a counting time $t = 8$ s). Phase analysis of X-ray diffraction patterns of BST60/40 thin films grown on stainless steel substrates was carried out using Match! (Crystal Impact) computer program.[8] The structural analysis was performed with X'pert HighScore Plus software (PANalytical B.V). The latest available ICSD,[9] ICDD[10] and IUCr/COD/AMCSD,[11] databases were utilized. Refinement of the structural parameters of BST60/40 thin films was performed with the Rietveld method.[12]

Microstructure of the BST60/40 thin films was studied by atomic force microscopy (AFM). Visualization and calculations were performed with a program module for processing and analysis of SPM images and SPM data by NT-MDT.[13]

For electric measurements, the upper surface of the thin films was covered with silver electrodes by sputtering technique through a shadow mask so as to define capacitors for electrical testing. The tool of the impedance spectroscopy was used to study dielectric properties of BST60/40 thin films at low frequencies (10 Hz–1 MHz, Solartron) at room temperature.

3. Results and Discussion

3.1. *Thermal behavior of the BST60/40 dry gel*

Simultaneous thermal analysis (STA) in which both thermal analysis (DTA) and mass change effects (TG) are measured concurrently on the same sample was used to investigate thermal effects in the dry gel of BST60/40 composition. Results of the thermal analysis were reported in detail elsewhere.[14] Let us only briefly mention that dried gel powder

exhibited a large total mass loss $\Delta m = 47\%$. The analysis shows three stages of the mass loss. The first drop on the TG curve of about $\Delta m_1 \approx 15\%$ occurred below $T = 300°$C and corresponded to the evaporation of the solvent. The second notable mass loss $\Delta m_2 \approx 21\%$ was detected at $T \approx 337°$C. The mass loss was probably due to the decomposition of organic additives in the gel. The third notable drop visible between $T = 600°$C and 800°C was likely originated from the release of various side products during alcoxolation and oxolation.[14]

3.2. *Crystal structure and phase composition of BST60/40 ceramic thin film*

As an example, X-ray diffraction peaks of sol–gel deposited BST60/40 ceramic thin film grown on AISI-304-type stainless steel and fired at $T = 650°$C for 2 h are shown in Fig. 1 (see the upper plot labeled as Peak List). The bottom plot shows the diffraction peaks of the substrate (labeled as Iron Nickel). The peak positions of the reference patterns are also shown in Fig. 1.

The search-match procedure was performed after raw data processing. One can see from Fig. 1 that the experimental diffraction peaks match the phase of the chemical composition $Ba_{0.59}Sr_{0.41}TiO_3$. The visual inspection of the diffraction data has shown that three strong diffraction lines are due to additional phases, namely the substrate $2\Theta = 51.23^0$ and 59.85^0 and substrate holder $2\Theta = 34.13^0$ (second plot from the bottom).

Detailed structural analysis of X-ray diffraction patterns was performed with Rietveld method. A model structure of BST6040 phase (cubic symmetry, *Pm-3m*(221) space group) according to the ICSD database (code 90006) was taken as an initial structure for structural parameters refinement. Results of the calculations were performed for XRD profile modeled with a Pseudo-Voigt function. The following R-parameters were obtained: $R_p = 23.92\%$, $R_{wp} = 30.96\%$, $R_{exp} = 6.53\%$. Calculated density of the thin film material
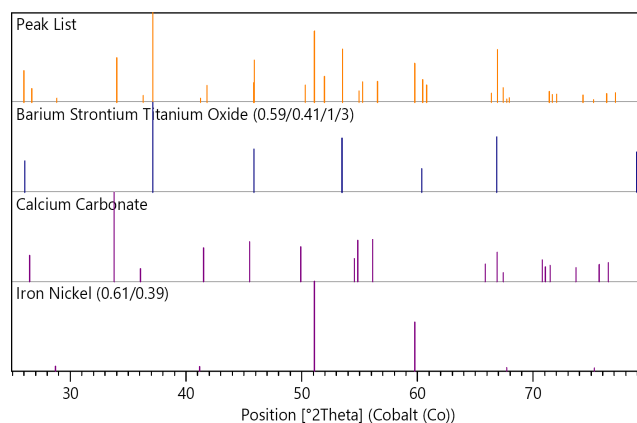

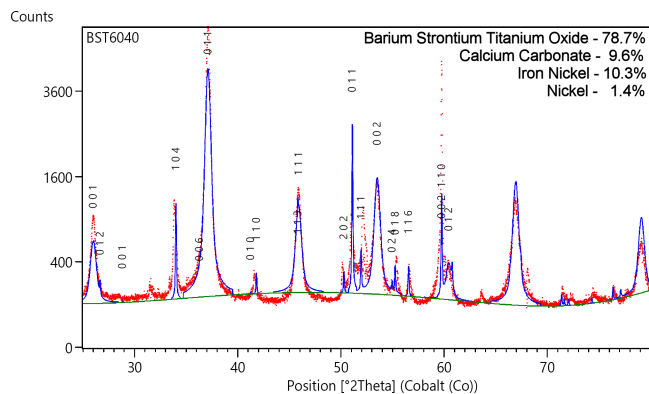Fig. 1. Identification of the phases in the sol–gel deposited BST60/40 thin film on stainless steel substrate.

Fig. 2. Results of the X-ray pattern fitting for BST6040 thin film.

was $\rho = 5.64$ g/cm^3 and calculated elementary cell parameter was $a = 3.971(8)$ Å.

Results of the X-ray pattern fitting for BST60/40 thin film on stainless steel substrate are given in Fig. 2.

3.3. *Morphology and piezoelectric response of BST60/40 thin films*

Microstructure of the BST thin films was studied by AFM. Morphology of the BST thin film surface of $60 \times 60\,\mu$m is shown in Fig. 3.

Statistical analysis of the surface roughness of $(Ba_{0.6}Sr_{0.4})TiO_3$ thin film deposited on stainless steel substrate have shown that average roughness of the thin films surface is $Sa = 55.55$ nm and root mean square, $Sq = 77.29$ nm. The histogram of the surface roughness is shown in Fig. 4, whereas the measured parameters and the data obtained are given as an inset in Fig. 4.

It is worth noting that the thin film was deposited on polished stainless steel of AISI-304 — type which was
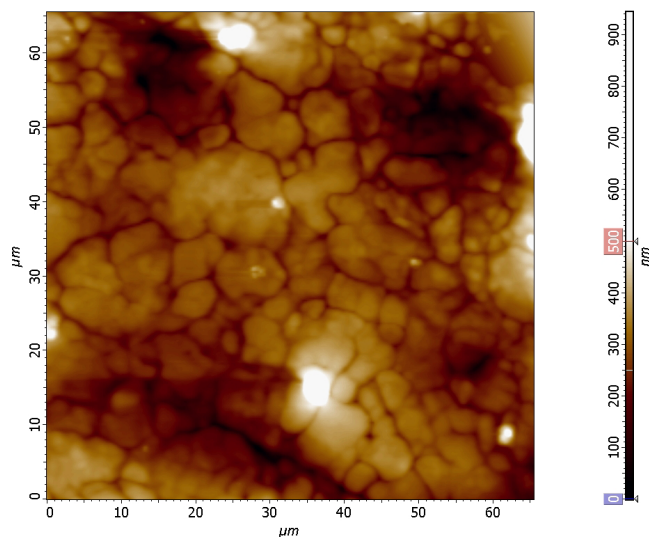

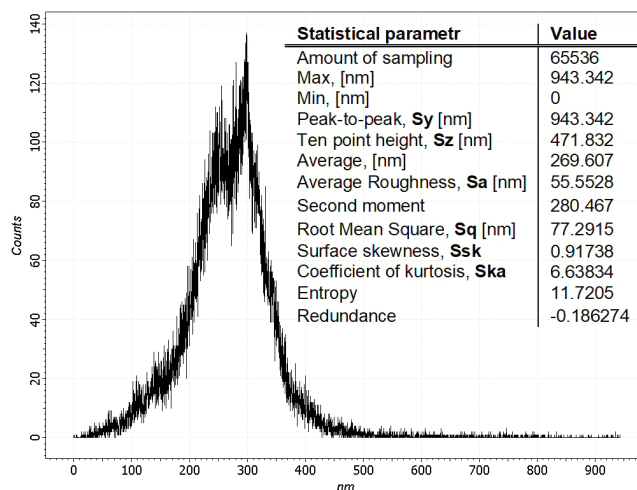Fig. 3. Topography of $(Ba_{0.6}Sr_{0.4})TiO_3$ thin film deposited on stainless steel substrate.

Fig. 4. Histogram characterizing the thin film surface roughness.

characterized with an arithmetic mean height of the surface $Sa = 0.05\,\mu$m. Therefore, one can conclude that the BST60/40 thin film surface mainly depended on the roughness of the substrate.

It is commonly known[15] that as structure dimensions are getting smaller, ferroelectrics exhibit a pronounced size effect manifesting itself in a significant deviation of the properties of low-dimensional structures from their bulk analogs. Recent advances in synthesis and fabrication of micro and nanoscale ferroelectrics brought to life new physical phenomena and devices that need to be studied and understood at this scale. Common AFM provides an ideal platform for local piezoelectric effect study due to high vertical resolution and high localization of electric field at the junction between the tip and the surface. Hence, piezoresponse force microscopy (PFM) is a contact-mode AFM in which an electrically-biased conductive AFM tip is used as a probe of local electromechanical coupling via the converse piezoelectric effect, which is a linear coupling between the electrical and mechanical properties of a material. PFM is based on the detection of local piezoelectric deformation of a ferroelectric sample induced by an external electric field (hence the name "piezoresponse").[16]

Results of the piezoelectric response measurements of BST60/40 thin films are shown in Fig. 5. One can see the correlation between topography (Fig. 3) and piezoelectric response — PFM (Fig. 5). An image of the thin film vertical piezoelectric response (Fig. 5) is of high contrast and make the visualization of the presence of ferroelectric domains in BST60/40 thin film possible at room temperature. The contrast corresponds to the value of piezoelectric current.

One can see in Fig. 5 relatively large areas characterized by different contrast. Dark area corresponded to current intensity ($I = -1.501$ nA) which was two times higher than that for the bright areas ($I = -0.748$ nA). As an example, profiles of the piezoelectric current measured along the two perpendicular lines, i.e., at coordinate $x = 30\,\mu$m and at coordinate $y = 30\,\mu$m are shown in Fig. 6.

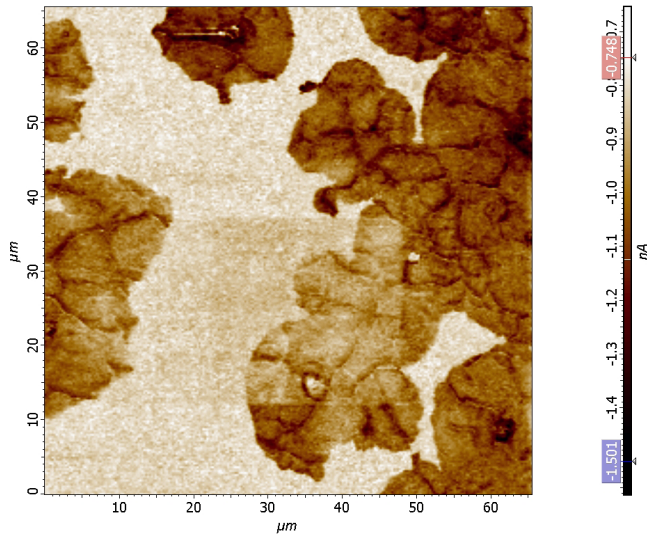Fig. 5. Piezoelectric response of $(Ba_{0.6}Sr_{0.4})TiO_3$ thin film deposited on stainless steel substrate.

It should be noted that to detect the polarization orientation, the PFM tip is used as a top electrode, which is moved over the sample surface. The electric field generated in the sample causes the domains with the polarization parallel to the field to extend and the domains with opposite polarization to contract. Therefore the method of measurement utilized in the present study made it possible to carry out only vertical PFM signal detection, the domain structure was of the $180°C$ — c type. One can see in Fig. 6 a fine current structure in a form of many local peaks and dips. This subtle structure may bear evidence of the domain structure of BST60/40 thin film.

As far as piezoelectric properties of BST60/40 thin film have been confirmed, it is truly justified that dielectric

response of the BST60/40 thin film should be analyzed with electric equivalent circuit typical for piezoelectric sample. Many researchers have developed equivalent impedance and electrical circuit models of piezoelectric materials based on electrical representation of the coupled electrical and mechanical problems. One of the traditional circuit models used for a piezoelectric resonator is Van Dyke's circuit model.[17]

To perform an analysis, the experimental data of impedance spectroscopy of BST60/40 thin films at low frequencies (10 Hz–1 MHz) studied by us earlier[5,18] were taken into consideration. The electric equivalent circuit used for thin film impedance data analysis is shown in Fig. 7. It consists of the piezoelectric loop ([L1R1C1]C0) — the Van Dyke's circuit[19] connected in series with two capacitance loops [(R2CPE2)(R3CPE3)] — the Voigt model.[20] In this connection two issues should be noted. First, the so called "Boukamp circuit description code"[21] was used in which the '(' and ')' brackets designate a parallel arrangement for the elements between the brackets, while the '[' and ']' set designates a series arrangement. Second, due to the distribution of relaxation times observed in solid materials, the capacitance C was replaced by a constant phase element (CPE), which represents more accurately the behavior of the grain interior, grain boundary and electrode processes.[20]

Experimental impedance data were fitted to the corresponding equivalent circuit (Fig. 7) using the complex nonlinear least squares method (CNLS).[22] Parameters of the equivalent electric circuit are given in Table 1.

Results of the fitting are plotted in Fig. 8 as a Bode-type plot. One can see a very good agreement between the experimental and fitted values.

The quality of the parameter fit of an equivalent circuit to a set of impedance data can be best seen in a fit quality plot (FQ-plot) in which the relative deviations of the real, ΔRe,
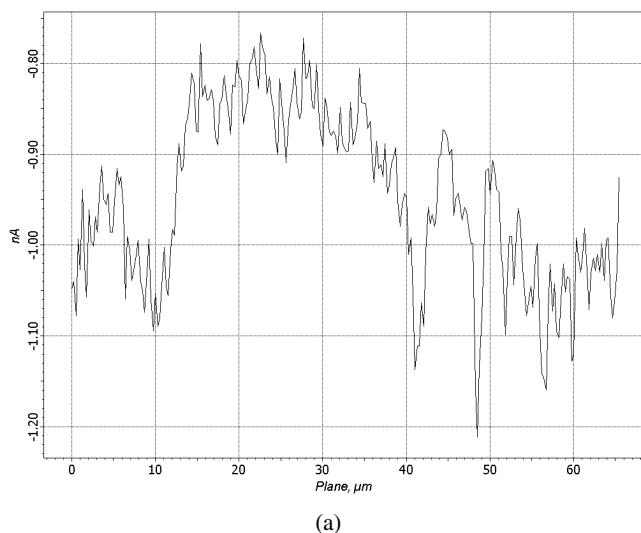
(a)
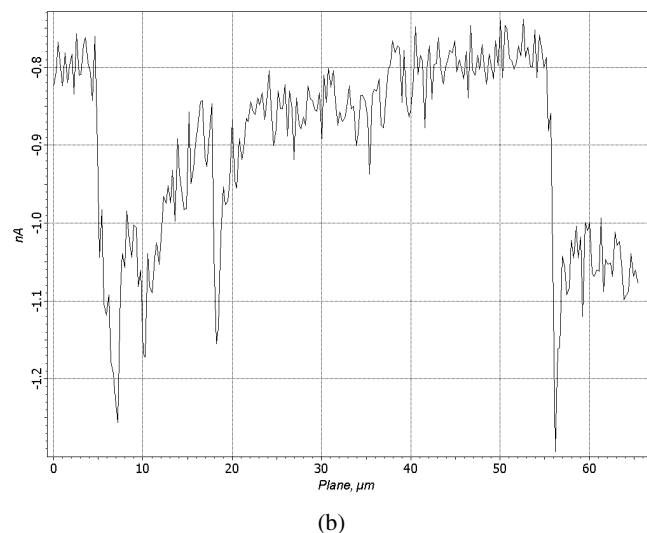
(b)

Fig. 6. Piezoelectric current measurements. The current was measured along the horizontal line at coordinate $y = 30\,\mu m$ (a) and along a vertical line at coordinate $x = 30\,\mu m$ on the piezoresponse image shown in Fig. 5.
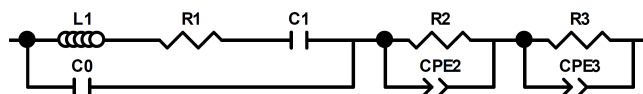
Fig. 7. Equivalent electric circuit.

Table 1. Estimated values of resistance (R_i), capacitance (C_i), constant phase element parameters (CPE$_i$-T), (CPE$_i$-P); The validity of the fitting procedure was estimated by χ^2 and WSS.

Element	Value
L_1 [H]	0.11121
R_1 [Ω]	3.5113×10^5
C_1 [F]	2.9353×10^{-7}
C_0 [F]	1.2259×10^{-11}
R_2 [Ω]	4.987×10^6
CPE$_2$-T [1/Ω]	6.9997×10^{-12}
CPE$_2$-P [1]	0.94586
R_3 [Ω]	1.9217×10^6
CPE$_3$-T [1/Ω]	3.0398×10^{-10}
CPE$_3$-P [1]	0.78847
Chi-Squared (χ^2),[1]	0.002281
Weighted Sum of Squares (WSS),[1]	0.43795

and imaginary part, ΔIm, of the impedance are plotted against frequency (ν) on a log scale.

For a good fit, these deviations should be distributed randomly around the frequency axis. One can see from Fig. 9 that the distribution can hardly be taken as a "white noise"/. However, only at the limits of the measuring frequency, residuals exceed a value of ~3%. Moreover, taking into consideration that the spectroscopic plot of the phase angle θ of the complex impedance Z is a very sensitive parameter of the goodness, we can conclude that the results obtained are of good quality.

On the base of the estimated fitting data (given in Table 1), the simulation of the impedance response of particular loops of the electric equivalent circuit was performed and the results are shown in Fig. 10.

One can see from Fig. 10 that the contribution of the "piezoelectric loop" of the equivalent circuit into the total
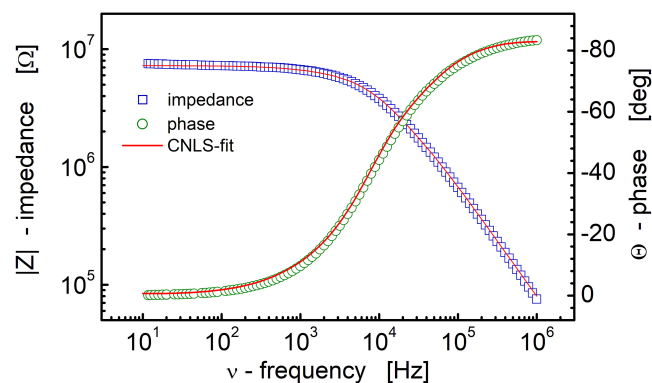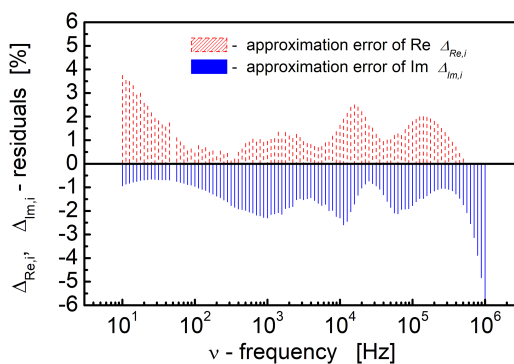

Fig. 9. FQ-plot for the final parameter set obtained with the dispersion analysis program for BST60/40 thin film.
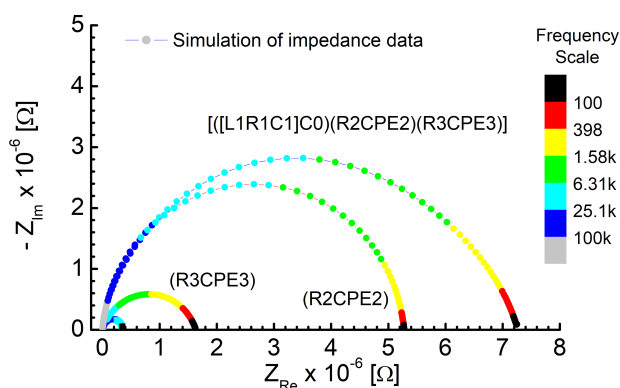

Fig. 10. Simulation of the impedance response of particular loops of the equivalent electric circuit shown in Fig. 7.

impedance response of the BST60/40 thin film at room temperature is not "high" (see: the smallest arc situated near at the origin of the impedance plot), however it cannot be neglected in the analysis. It is a common knowledge[23] that when overlapping between processes that increase, one may need alternative representations such as those based on combined spectroscopic plots of the imaginary components of impedance, "Z" and electric modulus "M" that highlights the phenomena with the largest resistance or picks out those with smallest capacitances. In case of the present studies, an alternative presentation of the impedance data in terms of imaginary component of electric modulus have shown a significant contribution of the "piezoelectric loop" of the equivalent circuit into the total dielectric response of the object under studies.

On the base of (R_iCPE$_i$), loops of the equivalent circuit (Fig. 7) resistance (R_i), capacitance (C_i), and relaxation frequencies (ω_{max}) were calculated and the results are given in Table 2.

One can see from Table 2 that, apart from "piezoelectric loop," two relaxation processes were identified and deconvoluted from the total impedance response by the electric equivalent circuit method and CNLS fitting procedure. One of the processes is characterized by the angular relaxation

Fig. 8. CNLS fitting of the impedance data with electric equivalent circuit: [([L1R1C1]C0)(R2CPE2)(R3CPE3)].

Table 2. Resistance (R_i), capacitance (C_i), and relaxation frequencies calculated on the base of (R_iCPE$_i$) circuits.

Element	Value
R_2 [Ω]	5.2773×10^6
C_2 [F]	3.761×10^{-12}
ω_{2max} [rad/s]	50136
Depression angle β_2 [$^\circ$]	5.6824
R_3 [Ω]	1.6339×10^6
C_3 [F]	5.3592×10^{-11}
ω_{3max} [rad/s]	10807
Depression angle β_3 [$^\circ$]	18.866

frequency $\omega_{2max} = 50136$ rad/s and the capacitance value $C_2 = 3.761 \times 10^{-12}$ F. Taking into consideration typical capacitance values for relaxation processes,[24] one may ascribe it to the bulk relaxation processes. In this connection, it is worth noting that in case of well-resolved bulk and grain boundary terms, one may expect that the grain boundary relaxation processes will exhibit one or two orders of magnitude of smaller relaxation frequency than the bulk relaxation frequency. In this study, however, the second of the relaxation processes exhibited smaller relaxation angular frequency but of the same order of magnitude namely, $\omega_{3max} = 10807$ rad/s. Nevertheless, taking into consideration the differences in amplitude of the grain boundary arc (see Fig. 10), high depression angle of the grain boundary arc ($\beta_3 = 18.87^\circ$) and one order of magnitude of higher capacitance value $C_3 = 5.3592 \times 10^{-11}$ F — one may ascribe relaxation frequency to grain boundary processes.

4. Conclusions

By means of sol–gel method followed by thermal processing, BST6040 electroceramic thin film was successfully fabricated. It was found that BST60/40 thin film adopted the cubic crystal structure described as *Pm-3m*(221) with an elementary cell parameter $a = 3.971(8)$ Å.

Statistical analysis of the thin film roughness showed that average roughness is characterized with a parameter Sa = 55.55 nm. Taking into consideration that the BST60/40 thin film was deposited on stainless steel substrate with Sa = 50 nm, one can conclude that the roughness of the sol–gel deposited thin film depended on the quality of the polished surface of the substrate.

Results of investigation of functional properties of the BST60/40 thin films have shown a subtle structure of piezoresponse signal in a form of many local peaks and dips. This subtle structure of "piezoelectric current" may bear evidence of the local piezoelectric deformations of BST60/40 thin film at room temperature.

The dielectric behavior of $Ba_{0.60}Sr_{0.40}TiO_3$ thin film was modeled successfully using an equivalent electrical circuit consisting of a series connection of three loops namely, a parallel combination of a capacitor and R, L, C elements connected in series (the Van Dyke's circuit) to model the piezoelectric response, a parallel combination of a resistor and constant phase element connected in series (the Voigt's circuit) to model the response of the grain interior and/or grain boundary. It was found that although "piezoelectric loop" had the smallest contribution to the total dielectric response, it could not be neglected in the analysis.

References

[1] K. H. Hellwege and A. M. Hellwege (eds.), *Complex Perovskite-type Oxides, Landoldt-Börnstein: Oxides*, Vol. 16a (Springer-Verlag, Berlin, Heidelberg, New York, 1981).

[2] E. Nakamura and T. Mitsui (eds.), *Complex Perovskite-type Oxides, Landoldt-Börnstein: Oxides*, Vol. 28 (Springer-Verlag, Berlin, Heidelberg, New York, London, Paris, Tokyo, Hong Kong, 1990).

[3] R. Waser (ed), *Nanoelectronics and Information Technology* (Wiley-VCH, Weinheim, 2005).

[4] B. Jaffe, W. R. Cook and H. Jaffe, *Piezoelectric Ceramics* (Academic Press, London, 1971).

[5] D. Czekaj, *Fabrication and Study of BST-based Functional Materials* (University of Silesia, Gnome Publishing House, Katowice, 2010), p. 122.

[6] A. Tumarkin, S. Razumov, A. Odinets, A. Gagarin, A. Altynnikov and A. Kozyrev, Ferroelectric BaSrTiO₃ films structured by an intermediate annealing during the deposition, *Integr. Ferroelectr.* **173**, 38 (2016).

[7] A. Tumarkin, A. Gagarin, A. Odinets, M. Zlygostov, E. Sapego and I. Kotelnikov, Structural and microwave characterization of BaSrTiO₃ thin films deposited on semi-insulating silicon carbide, *Jpn. J. Appl. Phys.* **57**, 11UE02 (2018).

[8] MATCH! Version 2.0.11, CRYSTAL IMPACT, Postfach 1251, 53002 Bonn, Germany, http://www.crystalimpact.com/match.

[9] ISCD Database, FIZ Karlsruhe, http://www.fiz-karlsruhe.de.

[10] International Centre for Diffraction Data, 12 Campus Boulevard, Newton Square, PA 19073–3273 U.S.A.; http://www.icdd.com.

[11] IUCr/COD/AMCSD Database, http://www.crystalimpact.com.match.

[12] H. M. Rietveld, The rietveld method-a historical perspective, *Austr. J. Phys.* **41**(2), 113 (1988).

[13] NOVA 1.0.26 2004 NT-MDT, http://www.ntmdt.com.

[14] K. Osinska and D. Czekaj, Thermal behavior of BST//PVDF ceramic–polymer composites, *J. Therm. Anal. Calorim.* **113**, 69 (2013).

[15] A. Gruverman and A. Kholkin, Nanoscale ferroelectrics: Processing, characterization and future trends. *Rep. Prog. Phys.* **69**, 2443 (2006).

[16] D. Seol, B. Kim and Y. Kim, Non-piezoelectric effects in piezoresponse force microscopy, *Curr. Appl. Phys.* **17**, 661 (2017).

[17]C. H. Park, On the circuit model of piezoceramics, *J. Intelli. Mater. Syst. Struc.* **12**, 515 (2001).

[18]D. Czekaj, A. Lisińska-Czekaj, T. Orkisz, J. Orkisz and G. Smalarz, Impedance spectroscopic studies of sol–gel derived barium strontium titanate thin films, *J. Eur. Ceram. Soc.* **30**, 465 (2010).

[19]K. S. Van Dyke, The electric network equivalent of a piezoelectric resonator, in *Physical Review*. Vol. 25, American Institute of Physics (1925), p. 895A.

[20]A. Lasia, Electrochemical impedance spectroscopy and it's applications. *Modern Aspects of Electrochemistry*, (eds.) B. E. Conway, J. Bockris and R. E. White, Vol. 32 (Kluver Academic/ Plenum Publishers, New York, 1999), pp. 143–248.

[21]B. A. Boukamp, Electrochemical impedance spectroscopy in solid state ionics: Recent advances, *Solid State Ion.* **169**, 65 (2004).

[22]B. Boukamp, A nonlinearleast squares fit procedure for analysis of immitance data of electrochemical systems, *Solid State Ion.* **20**, 31 (1986).

[23]A. R. West, D. C. Sinclair and N. Hirose, Characterization of electrical materials, especially ferroelectrics, by impedance spectroscopy, *J. Electroceram.* **1**(1), 65 (1997).

[24]J. C. Ruiz-Morales, D. Marrero-Lopez, J. T. S. Irvine and P. Nunez, A new alternative representation of impedance data using the derivative of the tangent of the phase angle Application to the YSZ system and composites, *Mater. Res. Bull.* **39**, 1299 (2004).